Improving Assimilated Global Data Sets Using TMI Rainfall and Columnar Moisture Observations

Arthur Y. Hou, Sara Q. Zhang, Arlindo M. da Silva
Data Assimilation Office
NASA Goddard Space Flight Center

William S. Olson
Joint Center for Earth Systems Technology
University of Maryland, Baltimore County

Summary

Global data sets that optimally combine observations from diverse sources with physical models of atmospheric and land processes are useful for initializing weather and climate predictions and for monitoring and understanding the earth systems. Such data sets currently contain significant errors in primary hydrological fields such as precipitation and evaporation, especially in the tropics. Our study shows that assimilation of rain rates and the total precipitable water (TPW) derived from the TRMM Microwave Imager (TMI) improves not only the hydrological cycle but also key climate parameters such as clouds, radiation, and the circulation in the analysis produced by the Goddard Earth Observing System (GEOS) data assimilation system.

Diagnostics reveal that rainfall assimilation reduces state-dependent systematic errors in clouds and radiation in regions of active convection, while TPW assimilation reduces errors in the moisture field to improve the radiation in clear-sky regions. The improved analysis also yields better short-range forecasts in the tropics, although these improvements are not as substantial as the improvements in the monthly-averaged assimilated data products. Overall, this study demonstrates the immense potential of using high-quality space-borne rainfall and moisture observations from microwave instruments to improve the quality of assimilated global data for climate analysis and weather prediction applications.

Improving Assimilated Global Data Sets Using TMI Rainfall and Columnar Moisture Observations

Arthur Y. Hou, Sara Q. Zhang[+], Arlindo M. da Silva

Data Assimilation Office, Laboratory for Atmospheres
NASA Goddard Space Flight Center, Greenbelt, MD 20771

William S. Olson

Joint Center for Earth Systems Technology
University of Maryland Baltimore County, Baltimore, MD

September 7, 1999

(*Journal of Climate*)

[+] Also affiliated with General Sciences Corp., a subsidiary of Science Applications International Corp.

Corresponding author address: Dr. Arthur Y. Hou, Code 910.3, NASA Goddard Space Flight Center, Greenbelt, MD, 20771. E-mail: arthur.hou@gsfc.nasa.gov

Abstract

A global analysis that optimally combine observations from diverse sources with physical models of atmospheric and land processes can provide a comprehensive description of the climate systems. Currently, such data products contain significant errors in primary hydrological fields such as precipitation and evaporation, especially in the tropics. In this study we show that assimilating precipitation and total precipitable water (TPW) retrievals derived from the TRMM Microwave Imager (TMI) improves not only the hydrological cycle but also key climate parameters such as clouds, radiation, and the large-scale circulation produced by the Goddard Earth Observing System (GEOS) data assimilation system (DAS). In particular, assimilating TMI rain rates improves clouds and radiation in areas of active convection, as well as the latent heating distribution and the large-scale motion field in the tropics, while assimilating TMI TPW retrievals leads to reduced moisture biases and improved radiative fluxes in clear-sky regions.

The improved analysis also improves short-range forecasts in the tropics. Ensemble forecasts initialized with the GEOS analysis incorporating TMI rain rates and TPW yield smaller biases in tropical precipitation forecasts beyond 1 day and better 500 hPa geopotential height forecasts up to 5 days.

Results of this study demonstrate the potential of using high-quality space-borne rainfall and moisture observations to improve the quality of assimilated global data for climate analysis and weather forecasting applications.

1. Introduction

Global reanalyses are useful in a variety of earth science applications but currently have order-one errors in primary fields of the hydrological cycle such as precipitation and evaporation, especially in the tropics (WCRP 1998, Adler et al. 1996). These errors limit the utility of these data for understanding the hydrological cycle and its role in climate variability. One way to improve estimates of these hydrological parameters is to assimilate new types of observations such as precipitation and the total precipitable water (TPW) to directly constrain these fields in the analysis. Assimilated global data that reliably capture tropical rainfall and latent heating distributions would provide valuable insights into the linkage between tropical convection and global energetics, and more specifically, the coupling between the hydrological cycle, atmospheric dynamics, and climate feedback. Given the crucial role of tropical latent heating in global climate and the sparse conventional observations in tropical regions, an important first step in improving global analyses is to ensure that the temporal and spatial variabilities of tropical rainfall are accurately represented.

The U.S.-Japan Tropical Rainfall Measuring Mission (TRMM) satellite launched in November 1997 provides, for the first time, cross-calibrated rain-rate estimates from a space-borne precipitation radar (PR) and a passive microwave instrument, the TRMM Microwave Imager (TMI). In this study we investigate the use of TRMM precipitation and TPW observations in global data assimilation and the extent to which assimilating these data improves the analysis produced by the Goddard Earth Observing System (GEOS) Data Assimilation System (DAS).

The Data Assimilation Office at the NASA Goddard Space Flight Center has been experimenting a "1+1" dimension variational algorithm based on a 6-hr time integration of a vertical column version of the GEOS DAS to assimilate surface rainfall and TPW observations. The basic methodology is described in Hou et al. (1999a), which showed that assimilating tropical precipitation and TPW observations derived from the Special Sensor Microwave Image (SSM/I) instruments aboard the polar-orbiting Defense Meteorological Satellite Program (DMSP) satellites improves not only the precipitation and moisture fields but also key climate parameters linked to convective activities such as the outgoing longwave radiation (OLR), clouds, and surface radiation in the GEOS analysis. These results demonstrated that these data are useful even

in sub-optimal applications without knowing their error characteristics and that physical parameterizations in the GEOS model have sufficient fidelity to capitalize on using these data.

In this article we report on the impact of assimilating TMI-derived surface precipitation and TPW retrievals on analyses produced by a 2° lat by 2.5° long by 46 model level version of the GEOS DAS using a slightly improved 1+1D algorithm. We plan to assimilate TRMM PR rainfall products at a later date using a higher resolution GEOS DAS.

The quality and utility of reanalyses as climate data sets depend upon their ability to capture climate signals with quantitative accuracy. Observations of outgoing radiative fluxes at the top of the atmosphere (currently not assimilated in the GEOS DAS) provide an independent measure of the overall quality of the GEOS assimilation data products. Radiation measurements from the Clouds and Earth's Radiation Energy System (CERES) instrument aboard the TRMM satellite will be used as a key verification data set. We will also compare clear and cloud-cleared brightness temperatures from spectral channels of the TIROS Operational Vertical Sounder (TOVS) with synthetic brightness temperatures computed using the GEOS temperature and moisture fields to infer how rainfall and TPW assimilation affects the upper tropospheric humidity and the tropospheric circulation and temperature.

Section 2 describes the 6-hr averaged, gridded TMI rainfall and TPW data sources. Section 3 gives a brief summary of the 1+1D assimilation scheme used in Hou et al. (1999a) and the further refinements adopted in the present study. Section 4 describes the assimilation experiments. Sections 5 and 6 examine the impact of TMI rainfall and TPW assimilation on the monthly-mean fields and short-range forecasts, respectively. Section 7 summarizes the main findings of this study.

2. Precipitation and TPW Observations

a. TMI GPROF precipitation retrieval

The TMI rain rates we use are physical retrievals using the Goddard Profiling (or GPROF) Algorithm, one of the operational algorithms resident at the TRMM Science Data and Information System (TSDIS). The algorithm obtains rain rates and precipitation vertical structure

from microwave radiometer and/or radar measurements (Kummerow et al. 1996, Olson et al. 1996) using a Bayesian technique similar to the algorithms developed by Pierdicca et al. (1996) and Haddad et al. (1997). The GPROF scheme uses a database of simulated precipitation vertical profiles and the associated microwave radiances generated by cloud-resolving model coupled to a radiative transfer code. This database serves as a "reference library" to which actual sensor-observed radiances can be compared. Given a set of multichannel radiance observations from a particular sensor, the entire library of simulated radiances is scanned; the "retrieved" profile is a composite using profiles stored in database which correspond to simulated radiances consistent with the observed radiances. For assimilation into the GEOS DAS, the single-footprint, instantaneous GPROF TMI surface rain rates are horizontally averaged to 2° lat. by 2.5° long. grids, which are then time-averaged over 6 hours centered at analysis times (0, 6, 12, 18 UTC).

The random error of each GPROF-retrieved rain rate may be estimated by evaluating the local variance of rain rates in the model database about the retrieved rain rate (Olson et al. 1996). According to this method, the random error of single-footprint, instantaneous rainfall rates is estimated to be ~100% of the retrieved rain rate. Over each 2° x 2.5° GEOS model gridbox, approximately 1000 single-footprint estimates from TMI are used to compute the area-average, instantaneous rain rate. Following the analysis of Bell et al. (1990), the corresponding random error of the gridbox-averaged TMI rain rate is about 20%. Undersampling of the time-average rain rate over each 6-hour analysis interval contributes additional error, approximately 20-60%, depending upon the number of TMI overpasses within the interval. One complication in this estimate is that the relative (percent) random error varies roughly as the inverse square root of the rain rate, so that estimates of relative random errors significantly worse in light rain areas, but better in heavy rain areas (Huffman 1997).

The global bias is not yet established for TMI GPROF rainfall estimates since most regions lack the necessary validation data and no statistical model has been developed to estimate bias from other parameters. On the monthly timescale, a recent intercomparison of TMI GPROF and coincident space-borne Precipitation Radar estimates of rain rate suggests biases on the order of 15% over land and 25% over ocean (S. Yang, personal communication).

b. TMI Wentz total precipitable water retrieval

The TPW are retrieved from TMI observations over oceans using essentially the same Wentz algorithms as those used for SSM/I TPW retrieval (Wentz 1997), except for adjustments to account for small differences in GHz between the TMI and SSM/I channels and the TMI water vapor being measured at 21 GHz rather than 22.235 GHz as in SSM/I. The TMI TPW data are available online from the Remote Sensing System (RSS 1999) in the form of maps of ascending and descending orbit segments between 40°S and 40°N at a pixel resolution of 25 km. The rms accuracy of the TMI TPW estimates is expected to be comparable or better than that of the SSM/I TPW retrieval, which is about 1 mm. These high-resolution data with good quality flags are then processed to produce 6-hour average 2° x 2.5° gridded TPW data for ingestion into the GEOS DAS.

3. The 1+1D Assimilation Algorithm

The algorithm we use to assimilate precipitation and TPW is an assimilation procedure in "1+1" dimensions based on a 6-hr time integration of a column version of the GEOS GCM with full model physics, with the advective terms prescribed from a preliminary 6-hr assimilation using conventional observations. Details of this 1+1D assimilation procedure and the basic features of the GEOS DAS are described in Hou et al. (1999a). The designation of "1+1D" refers to the involvement of both spatial and temporal dimensions to differentiate it from "2D" for 2 spatial dimensions. The procedure minimizes the least-square differences between the satellite-retrieved rain rates and the values generated by the column model averaged over the 6-hr analysis window. The control variables are analysis increments of moisture and temperature within the Incremental Analysis Update (IAU) framework of the GEOS DAS. The 1+1D scheme, in its generalization to four dimensions, is related to the standard 4D variational assimilation algorithm but differs in its choice of the control variable: instead of estimating the initial condition at the beginning of the assimilation cycle, it estimates the constant IAU forcing to be applied over a 6-hr assimilation cycle. In doing so, it also imposes the forecast model as a *weak constraint* in a manner similar to the variational continuous assimilation techniques (Derber 1989, Zupanski 1997).

An optimal use of TMI and SSMI rainfall and TPW observations in data assimilation

requires detailed knowledge of both observation and forecast model errors, which are currently research issues. It is meanwhile useful to understand the benefits of using these data in data assimilation in sub-optimal applications without error specifications, as done in Hou et al. (1999a). In this "perfect observation" limit, the explicit assumptions are: (i) that the observed rainfall and TPW estimates are much more reliable than the model-generated estimates, (ii) that uncertainties in the moisture field are much larger than and uncorrelated with errors in the temperature field, and (iii) that the moisture analysis increment has a known vertical structure. Under these conditions the general 1+1D scheme reduces to a two-parameter estimation problem to accommodate the 2 pieces of information provided by precipitation and TPW observations.

With the above simplifications, the 1+1D scheme shares a number of key assumptions with the physical initialization scheme (Krishnamurti et al. 1991, 1993).But the scheme as implemented in the GEOS DAS differs from physical initialization in an important respect - it is used to directly constrain the time-average rain rate and TPW over a 6-hr analysis window to match the observations, whereas the physical initialization scheme is used to improve the analysis through an improved first guess achieved by nudging the precipitation during the previous analysis cycle (Treadon 1996).

The detailed implementation of the 1+1D scheme in the "2-parameter, perfect-observation, moisture-adjustment" limit is described in Hou et al. (1999a). The vertical structure of the moisture analysis increment used in Hou et al. is define by a dimensionless parameter, $|\alpha| \leq 2$, that modifies the change in relative humidity as a linear slope adjustment to match the observed rain rate and a second parameter, β, for matching the observed TPW value. One drawback with this parameterization is that it leads to excessively large moisture increments aloft at locations of reduced precipitation. In the present work we obtain significantly better results by adopting a vertical structure function for the moisture analysis increment (i.e., Eq. (5) of Hou et al.) That mimics the Jacobian of the 6-hr mean precipitation w.r.t. moisture perturbations (see the Appendix). Substituting the moisture analysis increment over the 6-hr analysis window, $\Delta q(\alpha)$, (Eq. A4 of the Appendix) into definition of the cost function given by Eq. 4b of Hou et al. (1999a) defines a 1D minimization problem w.r.t. α for given observation values of P^o and $\bar{q}^o$: At each gridbox where the difference between the observed 6-hr rain rate, P^o, and the model-generated rain rate, P^f, exceeds 1 mm d^{-1}, we minimize the cost function given in Hou et al.; viz:

$$J(\Delta q(\alpha)) = [ln(P^o + \epsilon) - ln(P^f(\Delta q(\alpha)) + \epsilon)]^2 \quad (1)$$

where ϵ is a small constant used to prevent logarithmic singularity at zero rain rate (taken to be 0.01 mm d^{-1}). P^f is obtained from a 6-hr integration of the GEOS temperature and moisture equations updating only the moist physics terms with other tendencies prescribed from a preliminary global assimilation using all data types except precipitation (see Hou et al. for details). In this study, the minimization is performed within the range of $|\alpha| \leq 3$, which was chosen empirically. Expanding the search range can further reduce the error std dev's in the monthly-mean OLR and precipitation but could also degrade the 6-hr forecast of moisture against radiosonde data. The choice of $|\alpha| \leq 3$ yields significantly better monthly-mean OLR fields compared with results obtained using a linear Δr slope adjustment without degrading the 6-hr moisture forecast.

4. Assimilation Experiments

We performed three parallel assimilation experiments that extend from 1 December 1997 (soon after the TRMM launch) to 31 January 1998. The control is a standard GEOS assimilation with conventional observations, as described in Hou et al. (1999a). In two other cases, we assimilated, in addition to conventional observations, either the 6-hr averaged TMI rain rate (PCP assimilation) or the 6-hr TMI rain rate and TPW data (PCP+TPW assimilation). Since the CERES/TRMM daily, gridded ES-4 radiative flux measurements similar to the Earth's Radiation Budget Experiment (ERBE) products are not available prior to 1998 (CERES/TRMM 1998), the bulk of our analysis focuses on January 1998.

5. Impact on Time-Mean Fields

a. Surface precipitation

Figure 1 shows the impact of TMI rainfall and TPW assimilation on the monthly-mean

tropical precipitation for January 1998. Figure 1a is the observed precipitation as seen by the TMI. Figure 1b shows the discrepancy between the TMI rain rate and precipitation from the GEOS control sampled at TMI observation locations averaged over January. The corresponding errors for the TMI PCP assimilation and PCP+TPW assimilation are shown in Figs. 1c and 1d, respectively.

The monthly-mean spatial anomaly correlation (AC), bias, and error std dev w.r.t. the TMI data are indicated at the top of each panel, with the percentage changes relative to the GEOS control given in parentheses. Assimilation of TMI rain rates increases the anomaly correlation from 0.59 to 0.84, and reduces the error std dev by 27%. Assimilating the TMI TPW data with rain rates further increases the anomaly correlation to 0.88 and the std dev reduction to 31%.

The apparent increase in the time-mean tropical bias reflects the fact that the rainfall assimilation algorithm is more effective in reducing the precipitation intensity than enhancing it in the GEOS DAS. A plausible reason for this asymmetry is that enhancing precipitation requires moistening of the lower troposphere, but the high relative humidity in the tropical boundary layer limits, through saturation, the extent to which moisture analysis increments can moisten the low levels, while it allows a greater degree of drying to reduce precipitation. Such an asymmetry would account for the prevailing negative tropical bias in Figs. 1c and 1d, but the difference of 0.6 mm d^{-1} in the bias between Figs. 1d and the control (Fig. 1b) is comparable to observation uncertainties.

It is worth noting that the limited capacity of the 1+1D scheme in the GEOS DAS to match intense rain rates is especially noticeable in January 1998 due to the unusually intense rainfall observed in the Central Tropical Pacific at the peak of the El Niño. By comparison, the TMI-retrieved rain rates are generally weaker in December 1997 (not shown), in which case the precipitation in the GEOS control has a smaller bias in the tropics and the PCP+TPW assimilation yields a much closer match with the TMI observations.

b. Total precipitable water

Figure 2a shows Wentz's TMI TPW retrieval for January 1998. Figures 2b-d show the

monthly-mean differences between the TMI-sampled TPW from the three GEOS assimilations and TMI observations. Assimilating TMI rain rates without TPW data has only a small positive impact on TPW, mainly in reducing the tropical-mean bias. Figure 2d shows that assimilating TMI TPW retrievals virtually eliminates the monthly-mean spatial bias and reduces the error std dev by 73%.

c. *Validation using CERES/TRMM radiation measurements*

Since the GEOS DAS does not assimilate the observed outgoing longwave or shortwave radiation (OSR) fluxes, these measurements may be used to verify the overall improvement of the GEOS analysis from assimilating TMI rainfall and TPW observations. In this section we compare the OLR and OSR fields from GEOS analyses against the CERES/TRMM ERBE-like ES-4 gridded daily products.

Table 1 shows for January 1998 the time-mean spatial errors in OLR against CERES observations *for all tropical locations where the month-mean rainfall has been modified by more than 1 mm* d^{-1} as a result of assimilating TMI rain rates. Statistics show that TMI PCP+TPW assimilation increases the spatial anomaly correlation from 0.50 to 0.81, reduces the bias by 85% and the error std dev by 38%, with the bulk of the improvements coming from the use of TMI rain rates. In Table 2 similar statistics for the OSR show that assimilating TMI data increases the anomaly correlation from 0.50 to 0.81, the reduces the bias by 49%, and decreases the error std dev by 36%. Since errors in the OLR and OSR in the analysis are dominated by errors in clouds, these results are suggestive of substantial improvements of clouds over the raining regions. This is confirmed by the comparison of the infrared radiation "cloud forcing" (defined as the difference between clear-sky OLR and OLR) shown in Table 3.

Figures 3 and 4 show the improvements in the OLR and OSR over the entire tropical domain, respectively. Assimilating TMI rainfall and TPW data can reduce the error std dev in OLR by up to 35% and that in OSR by up to 24%. The tropical bias in OSR is dominated by errors in clouds in the GEOS DAS, and the use of TMI rainfall and TPW data systematically reduces this bias, as shown in Figs. 4c and 4d. In contrast to this, the tropical-mean OLR bias appears to increase as a result of assimilating TMI data (Figs. 3c and 3d). This apparent increase

is an artifact of the virtual elimination of the strong negative OLR bias in precipitating areas (as seen in Table 1), leaving the tropical-mean bias being dominated by the positive bias in the rain-free regions. The positive OLR bias in rain-free areas reflects a dry humidity bias in the lower troposphere, which is much reduced through the use of TPW observations, as shown by the comparison of the clear-sky OLR results against the CERES measurements in Table 4. The tropical bias in the clear-sky OSR is small in the GEOS control - about 1.02 Wm^{-2} (not shown). Rainfall and TPW assimilation reduces this bias to 0.90 Wm^{-2} (by roughly 12%) but does not affect the anomaly correlation or the error std dev.

One important benefit of assimilating rainfall and TPW data is that their use is effective in reducing state-dependent systematic errors in assimilation products. An example is given in Fig. 5, which compares the tropical-mean std dev errors in OLR from the GEOS control and the TMI PCP+TPW assimilation for three averaging periods of 1, 5, and 30 days. The offset between the control and PCP+TMI assimilation is effectively constant in all three cases ranging from 8.2 to 9.5 Wm^{-2}, signifying a reduction of state-dependent systematic errors since the tropical-mean bias has already been removed.

d. Validation using TOVS radiances

TOVS brightness temperature observations may be used to assess the impact of TMI rainfall and TPW assimilation on GEOS moisture and temperature analyses. We first compute "synthetic" TOVS brightness temperatures using temperature and humidity analyses from GEOS assimilations, and then compare them with brightness temperatures derived from the clear and cloud-cleared infrared radiances from the TOVS High-resolution Infrared Radiation Sounder 2 (HIRS2) and brightness temperatures from the TOVS Microwave Sounding Unit (MSU). The HIRS cloud-cleared brightness temperatures are from the Pathfinder Path A data set (Susskind et al. 1997). Details of the procedure are given in Hou et al. (1999a). In this section we examine results for 2 particular channels: The HIRS2 12 (6.7 μm), which is sensitive to the upper tropospheric humidity (UTH) and the MSU 2, which is sensitive to the mid-tropospheric temperature. As discussed in Hou et al., both the observations and radiative transfer calculation contain biases. The absolute uncertainty of the synthetic minus observed brightness temperatures

is estimated to be approximately 2 K. These biases were not removed. Instead, we concentrate on the spatial structure of the brightness temperature residuals exceeding 2 K and the relative differences between the GEOS control and PCP+TPW assimilations.

HIRS2 12 has a peak sensitivity to UTH between about 300 and 500 hPa depending on local conditions. Figure 6 compares the monthly-mean from the synthetic HIRS2 12 brightness temperature GEOS analyses with observation. Figure 6a shows that the synthetic brightness temperature of the GEOS control has a cold bias, indicative of a moist bias in UTH throughout the tropics. The difference in synthetic brightness temperature in Fig. 6b shows that TMI rainfall and TPW assimilation leads to "warming" over much of the tropics and small reductions in the spatial bias and the error std dev that are statistically significant. That these error reductions are further enhanced in experiments in which the TMI rainfall and TPW data are augmented by SSM/I observations (Hou et al. 1999b) suggest that they are meaningful. These results also confirm that the modified rainfall assimilation algorithm used in this study does correct the problem of excessive moistening aloft at locations of reduced precipitation found in Hou et al. (1999a). The spatial correlation between the warm brightness temperature anomaly in Fig. 6b and the area of negative specific humidity anomaly at 400 hPa in Fig. 6c is -0.65, while the correlation between the negative humidity anomaly and the positive (descending) omega velocity anomaly in Fig. 6d is -0.78. Thus the drying of the upper troposphere is directly linked to enhanced subsidence due to an improved tropical precipitation (aee section 5e).

The MSU 2 has a relatively broad sensitivity to tropospheric temperature that peaks near 600 hPa and has a small sensitivity to surface emission. Figure 7a shows that the monthly-mean synthetic MSU 2 brightness temperatures in the GEOS control are higher than the observed MSU 2 values, consistent with a warm bias in the temperature analysis. But these differences may not be significant since they are less than the overall uncertainty of about 2 K in brightness temperatures. We can remove this ambiguity by examining changes in the synthetic brightness temperatures between the two assimilation runs. Figure 7b shows that the impact of rainfall and TPW assimilation is to reduce the warm biases by 0.05 to 0.2 K over large portions of the tropics. Changes of this size may be significant given the broad weighting function and are consistent with the slightly reduced bias and std dev shown in Fig. 7b. In any case, there is no evidence of rainfall and TPW assimilation adversely affecting the tropospheric temperature.

e. Impact on the large-scale circulation and atmospheric energetics

Much of the improvements in the top-of-the-atmosphere radiation, upper tropospheric humidity shown in the previous sections are directly linked to improved clouds and large-scale motions due to improved precipitation and latent heating distribution through assimilation of TMI rain rates. Figure 8 shows the January-mean difference maps of precipitation, 200 hPa divergence wind vectors, 500 hPa omega velocity, OLR, and OSR between the TMI PCP+TPW assimilation and the control. Also shown are the spatial anomaly correlations between the change in precipitation and changes in these other fields; they range from -0.88 to 0.70. Clearly, an improved precipitation pattern has a direct impact on the horizontal distribution of clouds, which, in turn, improves the OLR and OSR. A better latent heating field affects not only the vertical motion in precipitating areas but also the large-scale horizontal divergence and the subsidence in surrounding regions leading to the improved UTH (see Figs. 6c and 6d). However, the impact of the large-scale circulation on the UTH in clear-sky regions, though positive, is small compared with the improvement due to TPW assimilation, as shown by the comparison of the clear-sky OLR results in Table 4.

6. Impact on Forecast

a. Precipitation forecast

Table 5 shows 6-hr average "observation minus forecast" (O-F) residuals for precipitation for lead times from 3 to 45 hours averaged over all tropical locations with available TMI observations. Forecasts were generated using initial conditions that were modified by TMI rainfall data in the previous assimilation window. Each ensemble consisted of forecasts from initial conditions 3 day apart over a 2-month period, which were treated as independent samples since convective precipitation has lifetimes on the order of hours. Bias and error std dev differences significant at the 99% level are italicized.

Results show that ensemble precipitation forecasts initialized by the PCP+TPW analysis have significantly smaller biases in 6-hr O-F residuals for forecast times greater than 9 hours. But

the improved initial condition using TMI rain rates and TPW data affects the error std dev of the 6-hr O-F residuals by only a few percent. In contrast to this, reductions in error std dev of the 6-hr "observation minus assimilation" (O-A) residuals are typically 15-30%. This shows that assimilating these data types using the 1+1D variational scheme can improve the analysis as a climate data set without necessarily requiring comparable improvements in the first guess (i.e., the 6-hr forecast). Nonetheless, it is of practical importance that assimilating these data types does not degrade the forecast since global analyses are routinely used to initialize forecast. Internal consistency between model physics and observations dictates that the improved analysis should also improve forecast, or at least, does not adversely affect forecast.

b. 6-hr observation minus forecast residuals

We computed the monthly-mean biases and error std dev's of the 6-hr O-F residuals for winds, geopotential height, and specific humidity averaged over tropical rawinsonde locations for the GEOS control and PCP+TPW runs. Statistical tests show that rainfall and TPW assimilation affects mainly the O-F residuals for moisture but not the winds. Table 6 gives the moisture O-F biases and std dev's along with the "null hypothesis" probabilities that they are the same between the two experiments. Results show that TMI rainfall and TPW assimilation leads to smaller std dev's of the moisture O-F residual between 300 and 500 hPa at the 1% probability level. The only significant changes in the biases occur between 700 and 850 hPa, corresponding to a downward displacement of the zero-bias level in the PCP+TPW case. The reduced moisture bias at 850 hPa is consistent with the use of TPW data but the robustness of the t-test result is questionable since the std dev's are not the same in the two cases according to the F-test. Apart from the impact on the moisture field, the only other notable change is a 61% reduction in the std dev of the O-F residual for the geopotential height at 400 hPa in the PCP+TPW case.

Taken together, these O-F results show that TMI rainfall and TPW assimilation tends to reduce the moisture O-F residuals with no adverse effect on other fields. This is consistent with the results from comparisons with TOVS brightness temperatures discussed in section 5d.

c. 5-day forecast

To analyze the impact of TMI rainfall and TPW assimilation on short-range forecast, we performed parallel ensemble forecasts initialized with GEOS analyses with and without TMI data. Each ensemble consists of 12 independent samples of 5-day forecasts with initial conditions 5 days apart taken from two months of assimilation. For forecast verification, we used two analyses: (i) the operational analysis from the European Center for Medium-Range Weather Forecasts (ECMWF) and (ii) the average of the GEOS control and PCP+TPW analyses. Although the PCP+TPW analysis compares better with satellite observations than the control, as shown in section 5, using the average of two analyses for verification removes biases associated with the initial conditions.

Figure 9 shows the averaged rms errors of 5-day ensemble forecast for the 500 hPa geopotential height. Assimilation with TMI rainfall and TPW data yields smaller rms errors regardless which analysis is used for verification. In either case, Student's t test confirms that the forecast error reductions in the tropics are significant at the 99% level beyond 1 day. Although the differences in the extratropics shown in Fig. 9b and 9c are not statistically significant, they show that the use of rainfall and TPW data does not degrade the forecast in the extratropics.

Similarly, rainfall and TPW assimilation also reduces the rms errors in the divergent component of zonal and meridional winds in the tropics, but the improvements are significant at the 95% level only within the first 24 hours.

7. Summary and Concluding Remarks

This study shows that TMI-derived rain rates and TPW estimates are useful for improving the representation of hydrological variables and atmospheric energetics in GEOS analysis. It shows that the 6-hr averaged TMI rainfall retrieval, at the current level of uncertainty in intensity, is capable of providing valuable pattern and intensity information to improve the quality of global analyses. In particular, assimilating these data is especially effective in reducing spatial errors in the monthly-mean precipitation, moisture, OLR and OSR fields, which increases the utility of these data for studying long-term climate variability.

Assimilating TMI rainfall and TPW reduces much of the state-dependent systematic errors in assimilated data products in the tropics. The overall impact of tropical rainfall assimilation is

to improve distributions of clouds and atmospheric radiation in areas of active moist convection, as well as the latent heating distribution and the associated large-scale circulation. The primary benefit of TPW assimilation is to reduce moisture biases to improve the longwave radiation in clear-sky regions. Results show that assimilating both types of observations lead to improvements in the vertical motion field and reduced humidity biases in the upper troposphere. The latter is established by comparing synthetic TOVS brightness temperatures computed using the GEOS analyses with and without TMI observations against TOVS observations.

Ensemble precipitation forecasts initialized with the GEOS analysis with TMI rainfall and TPW data have significantly smaller biases in the tropics for forecast times longer than 9 hours. The GEOS PCP+TPW analysis also produces better ensemble 5-day forecasts of the 500 hPa geopotential height and 2-day forecasts of the 200 hPa divergent winds in the tropics. Although the GEOS analysis with TMI rainfall and TPW data produces better short-range forecasts, it is worth noting that improvements in the time-averaged fields are even more significant. This suggests that, in the presence of biases and other errors of the forecast model, it is possible to improve the time-averaged "climate content" in the assimilated data without necessarily requiring comparable improvements in forecast skills.

This study demonstrates that assimilating TMI rainfall and TPW data can substantially improve assimilated data sets even in sub-optimal applications without error specifications. It is possible to make more effective use of these observations through error covariance modeling. Results of this study provide a baseline for testing the performance of error covariance models in a generalized rainfall and TPW assimilation scheme.

Given the limited spatial coverage of TRMM in a 6-hr window, TRMM observations alone cannot improve the precipitation analysis over the entire tropics. What we present here is a proof-of-concept demonstration of the potential of using rainfall and TPW observations from space-borne microwave instruments to improve global analyses. In Hou et al. (1999b) we show that augmenting the TMI rainfall and TPW data with observations derived from SSM/I instruments further enhances the improvements described in this paper. The proposed Global Precipitation Mission to deploy a constellation of satellites to provide global rainfall observations with improved temporal sampling could lead to major advances in upgrading the quality and utility of global analyses for climate research and numerical weather prediction applications.

Acknowledgments

It is a pleasure to acknowledge the support of this research by Dr. Ramesh Kakar, the TRMM Program Scientist, and Dr. Kenneth Bergman, Manager of Global Modeling and Analysis Program through NASA Grants 621-15-33-20, 622-24-27-20 and 291-04-15-20. We would also like to thank Joanna Joiner for providing the code for computing TOVS synthetic brightness temperatures.

APPENDIX

The vertical structure of the moisture analysis increment

We introduce a vertical structure function, $G(p)$, in the moisture analysis increment (i.e., eqn. (5) of Hou et al.) to mimic the Jacobian of the 6-hr mean precipitation w.r.t. moisture perturbations; i.e.,

$$\Delta q = q_s(T)\,\Delta r \qquad (A1)$$

where $q_s(T)$ is the saturation specific humidity and Δr, the change in relative humidity, is given by:

$$\Delta r = \begin{cases} G(p)\,[\,\alpha\, ln(p) + \beta\,] & for\ p > p^* \\ 0 & otherwise \end{cases} \qquad (A2)$$

where $G(p)$ is a prescribed Guassian function with a maximum at 1000 hPa and an e-folding width of 300 hPa. At locations with valid TPW observations, the vertically integrated column moisture increment may be determined from retrieval of TPW, $\bar{q}^o$, and the model first guess, $\bar{q}^f$:

$$\Delta\bar{q} \equiv \int_0^{p_s} \Delta q \frac{dp}{g} = \bar{q}^o - \bar{q}^f \qquad (A3)$$

Combining (1)-(3) yields a Δq as a function of a single parameter, α :

$$\Delta q(\alpha) = q_s(T)\,G(p)\left\{ \left[\, ln(p) - \frac{\overline{q_s G ln(p)}}{\overline{q_s G}} \,\right] \alpha + \frac{\Delta\bar{q}}{\overline{q_s G}} \right\}, \qquad for\ p > p^* \qquad (A4)$$

If TPW data are not used, $\Delta\bar{q}$ is set to zero, so that the moisture increment due to precipitation data introduces no net moisture source in a vertical column. This does not mean that $\bar{q}$ is

conserved during the assimilation cycle since moisture can be modified by convective processes (see Hou et al. 1999a).

REFERENCES

Adler, R., C. Kidd, M. Goodman, A. Ritchie,, R. Schudalla, G. Petty, M. Morrissey, and S. Greene, 1996: PIP-3 Intercomparison Results, Report of the PIP-3 Workshop, College Park, MD. [Available online from http://www.ghcc.msfc.nasa.gov/pip3].

Bell, T. L., A. Abdullah, R.L. Martin, and G.R. North, 1990: Sampling errors for satellite-derived tropical rainfall: Monte Carlo study using a space-time stochastic model. *J. Geophys. Res.*, 95, 2195-2205.

CERES/TRMM, 1998: CERES Data Products Catalog. Available online from http//:asd-www.larc.nasa.gov/ceres/trmm/ceres_trmm.html

Derber, J.C., 1989: A variational continuous assimilation technique. *Mon. Wea. Rev.*, 117, 2437-2446.

Haddad, Z. S., E. A. Smith, C. D. Kummerow, T. Iguchi, M. R. Farrar, S. L. Durden, M. Alves, and W. S. Olson, 1997: The TRMM 'Day-1' Radar/Radiometer Combined Rain-Profiling Algorithm, *J. Meteor. Soc. Japan*, 75, 799-809.

Hou, A.Y., D. Ledvina, A. da Silva, S. Zhang, J. Joiner, R. Atlas, G. Huffman, and C. Kummerow, 1999a: Assimilation of SSM/I-derived surface rainfall and total precipitable water for improving the GEOS analysis for climate studies. *Mon Wea. Rev.*, in press. [Available online from http://dao.gsfc.nasa.gov/DAO_people/hou].

-----, S. Zhang, A. da Silva, W. Olson, 1999b: Improving assimilated global data sets using TRMM and SSM/I-derived rainfall and columnar moisture observations. *Bull. Am. Met. Soc.*, submitted.

Huffman, G.J., 1997: Estimates of root-mean-square random error contained in finite sets of estimated precipitation. *J. Appl. Meteor.*, 36, 1191-1201.

Krishnamurti, T.N., J. Xue, H.S. Bedi, K. Ingles, and O. Oosterhof, 1991: Physical initialization for numerical weather prediction over the tropics. *Tellus*, 43AB, 53-81.

------, H.S. Bedi, and K. Ingles, 1993: Physical initialization using SSM/I rain rates. *Tellus*, 45A, 247-269.

Kummerow, C., W. Olson, and L. Giglio, 1996: A simplified scheme for obtaining precipitation

and vertical hydrometeor profiles from passive microwave sensors. *IEEE Trans. Geosci Remote Sensing*, 34, 1213-1232.

Olson, W.S., C.D. Kummerow, G.M. Heymsfield, and L. Giglio, 1996: A method for combined passive-active microwave retrievals of cloud and precipitation profiles. *J. Appl. Meteor.*, 35, 1763-1789.

Pierdicca, N., F. S. Marzano, P. Basili, P. Ciotti, G. d'Auria, and A. Mugnai, 1996: Precipitation retrieval from spaceborne microwave radiometers based upon multivariate analysis of simulated cloud-radiation datasets. *IEEE Trans. Geosci. Remote Sens.*, 34, 1-16.

Remote Sensing Systems (RSS), 1999: Description of TMI and SSM/I data products. Available online from http://www.ssmi.com, Remote Sensing Systems, Santa Rosa, Calif.

Susskind, J., P. Piraino, L. Rokke, L. Iredell, and A. Mehta, 1997: Characteristics of the TOVS pathfinder path A data set, *Bull. Am. Meteorol. Soc.*, 78, 1449-1472.

Treadon, R.E., 1996: Physical initialization in the NMC global data assimilation system. *Meteor. Atmos. Phys.*, 60, 57-86.

World Climate Research Program (WCRP), 1998: Proceedings of the First WCRP International Conference on Reanalyses. October 27-31, Silver Spring, MD, 461 pp.

Wentz F. J., 1997: A well-calibrated ocean algorithm for SSM/I, *J. Geophys. Res.*, Vol. 102, No. C4, 8703-8718.

Zupanski, D., 1997: A general weak constraint applicable to operational 4DVAR data assimilation systems. *Mon. Wea. Rev.*, 125, 2274-2292.

Table 1

Spatial statistics of GEOS OLR against CERES/TRMM ERBE-like ES-4 OLR averaged over tropical locations where the monthly-mean rainfall has been modified by more than 1 mm d^{-1} (January 1998)

	anomaly corr	bias (Wm^{-2})		error std dev (Wm^{-2})	
GEOS Control	0.5	-17.7	-	27.9	-
PCP Assimilation	0.76	-8.05	-55%	18.9	-32%
PCP+TPW Assimilation	0.81	-2.65	-85%	17.3	-38%

Table 2

Spatial statistics of GEOS OSR against CERES/TRMM ERBE-like ES-4 OSR averaged over tropical locations where the monthly-mean rainfall has been modified by more than 1 mm d^{-1} (January 1998)

	anomaly corr	bias (Wm^{-2})		error std dev (Wm^{-2})	
GEOS Control	0.5	32.6	-	33.9	-
PCP Assimilation	0.78	22.3	-32%	22.4	-34%
PCP+TPW Assimilation	0.81	16.5	-49%	21.7	-36%

Table 3

Spatial statistics of GEOS IR cloud forcing against CERES/TRMM ES-4 data averaged over tropical locations where the monthly-mean rainfall has been modified by more than 1 mm d^{-1} (January 1998)

	anomaly corr	bias (Wm^{-2})		error std dev (Wm^{-2})	
GEOS Control	0.38	26.4	-	26.2	-
PCP Assimilation	0.78	18.5	-30%	15.1	-42%
PCP+TPW Assimilation	0.80	10.4	-61%	14.6	-44%

Table 4

Spatial statistics of GEOS clear-sky OLR against CERES/TRMM ERBE-like ES-4 measurements (30°S to 30°N, January 1998)

	anomaly corr	bias (Wm^{-2})		error std dev (Wm^{-2})	
GEOS Control	0.81	10.3	-	5.58	-
PCP Assimilation	0.82	9.44	-8%	5.46	-2%
PCP+TPW Assimilation	0.88	8.36	-19%	4.77	-15%

Table 5

Observation Minus Forecast Statistics for Precipitation in the Tropics

Forecast Time	3 hr	9 hr	15 hr	21 hr	27 hr	33 hr	39 hr	45 hr
Sample Size	34062	34093	33564	33223	34000	34099	34030	33995
	bias							
Control	0.684	0.717	0.813	0.777	*1.308*	*1.217*	*1.085*	*0.969*
PCP+TPW	0.572	0.363	0.041	0.055	*0.729*	*0.741*	*0.614*	*0.665*
% change	-16%	***-49%***	***-95%***	***-93%***	***-44%***	***-39%***	***-43%***	***-31%***
t prob	0.311	***0.001***	***0.0***	***0.0***	***0.01***	***0.006***	***0.001***	***0.005***
	error std dev							
Control	*14.59*	*14.41*	*15.11*	14.84	14.49	13.35	14.77	14.12
PCP+TPW	*14.17*	*14.14*	*15.09*	14.89	14.30	13.21	14.68	13.94
% change	***-2.9%***	***-1.9%***	-0.1%	+0.3%	-1.3%	-1.0%	-0.6%	-1.3%
F prob	***0.0***	***0.0***	0.813	0.568	0.017	0.039	0.254	0.015

Table 6

Specific humidity O-F residuals against rawinsonde data

(30°S to 30°N, January 1998)

Pressure (hPa)	Bias			Error Std Dev		
	Control	PCP+TPW	t-test prob	Control	PCP+TPW	F-test prob
300	-0.084	-0.08091	0.59293	***0.08169***	***0.06434***	***1.652×10^{-4}***
400	-0.1566	-0.13091	0.14265	***0.22429***	***0.18029***	***3.611×10^{-4}***
500	-0.147	-0.13544	0.66783	***0.34639***	***0.2921***	***4.330×10^{-3}***
700	***0.0332***	***-0.17823***	***1.710×10^{-4}***	0.68698	0.63535	0.1921
850	***0.55907***	***0.2718***	***6.851×10^{-3}***	1.27771	1.14982	0.0877
1000	-0.9933	-0.87725	0.50283	1.36974	1.39154	0.8595

Figure captions

Figure 1. (a) Time-mean TMI GPROF precipitation for January, 1998. (b) Difference between TMI observation and precipitation from the GEOS control sampled at TMI observation locations. Positive and negative values are inidcated by solid and dash contours, respectively. Also shown are tropically-averaged spatial anomaly correlation (AC), bias, and error std dev. (c) Same as (b) but for the TMI PCP assimilation. The percentage change in error std dev relative to the control is shown in parentheses. (d) Same as (c) but for the TMI PCP+TPW assimilation.

Figure 2. (a) Time-mean TMI Wentz TPW retrieval for January, 1998. (b) Difference between TMI observation and TPW from the GEOS control sampled at TMI observation locations, together with tropical-mean spatial statistics. Positive and negative values are inidcated by solid and dash contours, respectively. (c) Same as (b) but for the TMI PCP assimilation. The percentage changes in bias and std dev relative to the control are shown in parentheses. (d) Same as (c) but for the TMI PCP+TPW assimilation.

Figure 3. (a) Time-averaged CERES/TRMM ERBE-like OLR for January, 1998. (b) Difference between CERES observation and OLR from the GEOS control with the same sampling, together with tropical-mean spatial statistics. Positive and negative values are inidcated by solid and dash contours, respectively. (c) Same as (b) but for the TMI PCP assimilation. Percentage changes in statistics relative to the control are shown in parentheses. See text for an explanation of the asterisk. (d) Same as (c) but for the TMI PCP+TPW assimilation.

Figure 4. (a) Time-averaged CERES/TRMM ERBE-like OSR for January, 1998. (b) Difference between CERES observation and OSR from the GEOS control with the same sampling, together with tropical-mean spatial statistics. Positive and negative values are inidcated by solid and dash contours, respectively. (c) Same as (b) but for the TMI PCP assimilation. Percentage changes in statistics relative to the control are shown in parentheses. (d) Same as (c) but for the TMI PCP+TPW assimilation.

Figure 5. Error std dev in tropically averaged OLR as a function of averaging periods of 1, 5, 10, 15, and 30 days for the first 30 days in January, 1998.

Figure 6. Synthetic HIRS2 channel 12 brightness temperature for January, 1998. (a) Control minus TOVS observation, with dashes indicating negative values. (b) Change in brightness temperature: PCP+TPW assimilation minus control. Percent changes in tropical-mean bias and error std dev are shown in brackets. Positive and negative values are inidcated by solid and dash contours, respectively. (c) Change in specific humidity at 400 hPa. The spatial correlation between negative humidity anomalies and positive brightness temperature anomalies in (b) is -0.65. (d) Corresponding change in the omega velocity at 400 hPa. The correlation between positive anomalies in omega velocity and negative humidity anomalies in (c) is -0.78.

Figure 7. Synthetic MSU channel 2 brightness temperature for January, 1998. (a) Control minus TOVS observation. (b) Change in brightness temperature: PCP+TPW assimilation minus control. Percent changes in tropical-mean bias and error std dev are shown in brackets. Positive and negative values are inidcated by solid and dash contours, respectively.

Figure 8. (a) Change in precipitation between PCP+TPW assimilation and the control for January, 1998. Superimposed are the changes in the horizontal divergent wind vector at 200 hPa. (b) Change in the omega velocity at 500 hPa. The correlation between this and the change in precipitation in (a) is -0.88. (c) Corresponding change in OLR. The correlation between this and the change in precipitation is -0.72. (d) Change in OSR. The correlation between this and the change in precipitation is 0.70.

Figure 9. Ensemble-mean rms error for 12 cases of 5-day forecasts of the 500 hPa geopotential height: Solid lines are results using the ECMWF analysis as verification. Dashes are same forecasts with the GEOS assimilation as verification.

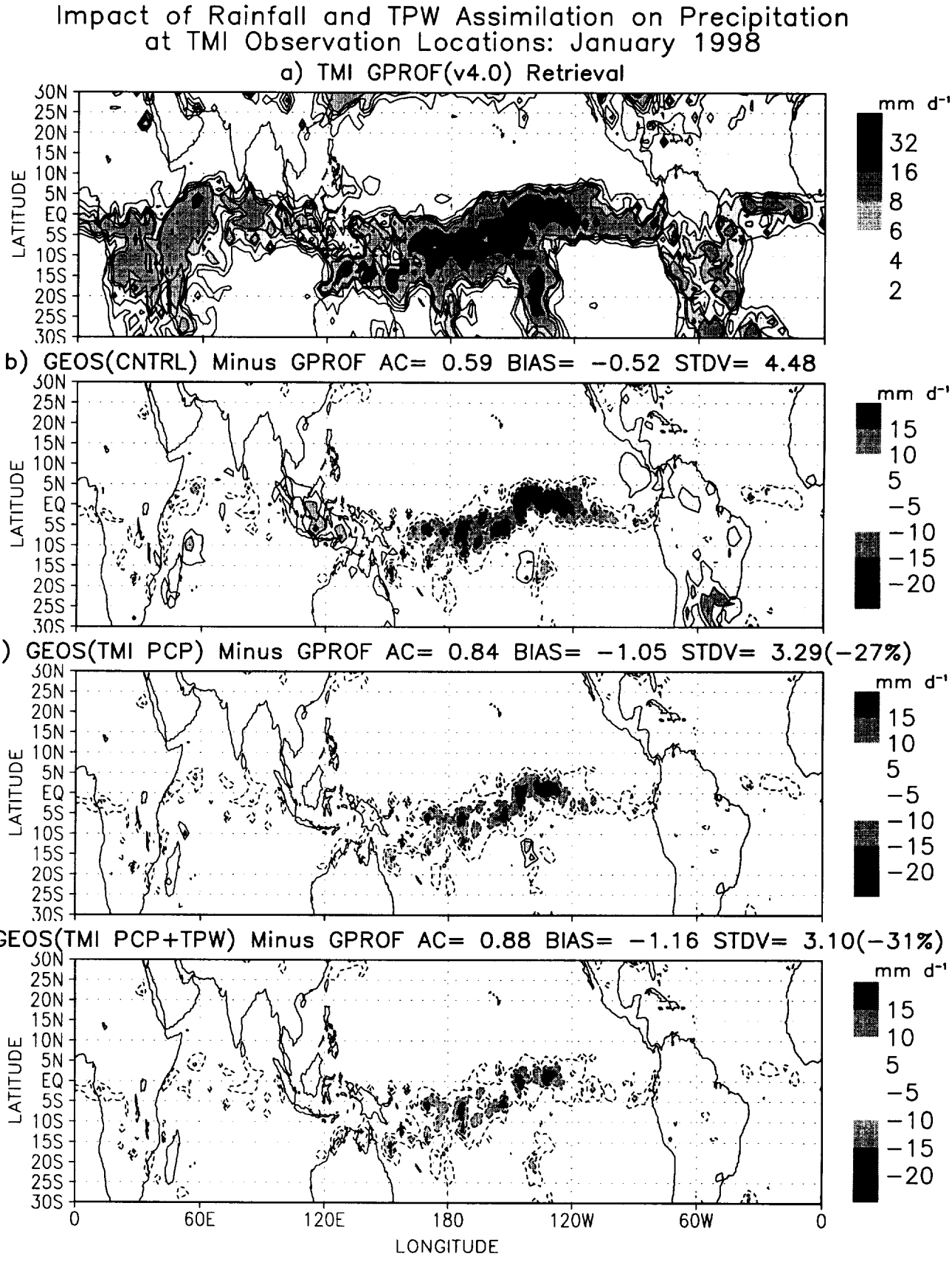
Impact of Rainfall and TPW Assimilation on Precipitation
at TMI Observation Locations: January 1998
a) TMI GPROF(v4.0) Retrieval
b) GEOS(CNTRL) Minus GPROF AC= 0.59 BIAS= −0.52 STDV= 4.48
c) GEOS(TMI PCP) Minus GPROF AC= 0.84 BIAS= −1.05 STDV= 3.29(−27%)
d) GEOS(TMI PCP+TPW) Minus GPROF AC= 0.88 BIAS= −1.16 STDV= 3.10(−31%)
LATITUDE
LONGITUDE
30N
25N
20N
15N
10N
5N
EQ
5S
10S
15S
20S
25S
30S
0
60E
120E
180
120W
60W
mm d⁻¹
32
16
8
6
4
2
15
10
5
−5
−10
−15
−20

Fig. 1

Impact of Rainfall and TPW Assimilation on TPW: January 1998

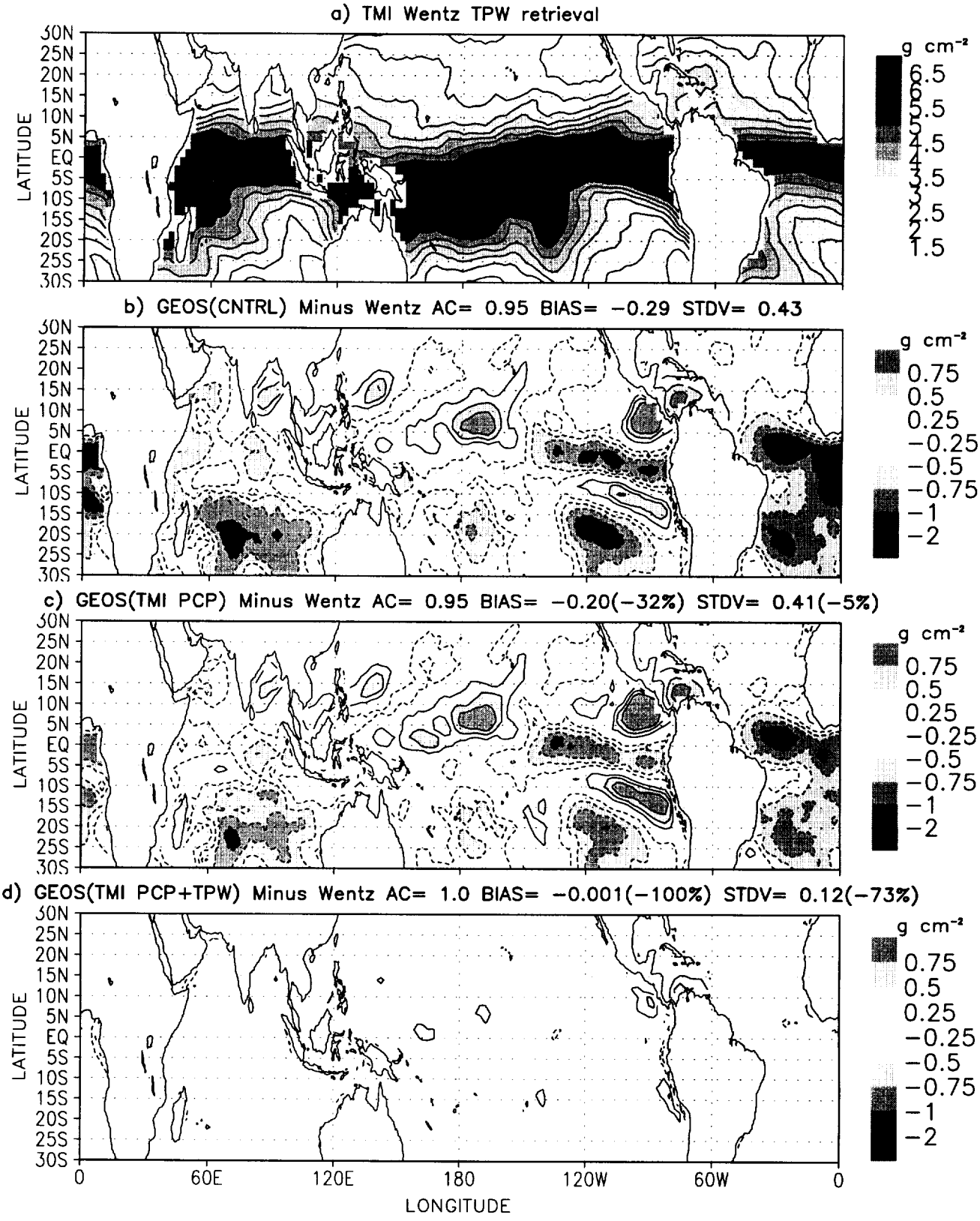

Fig. 2

Impact of Rainfall and TPW Assimilation on OLR: January 1998

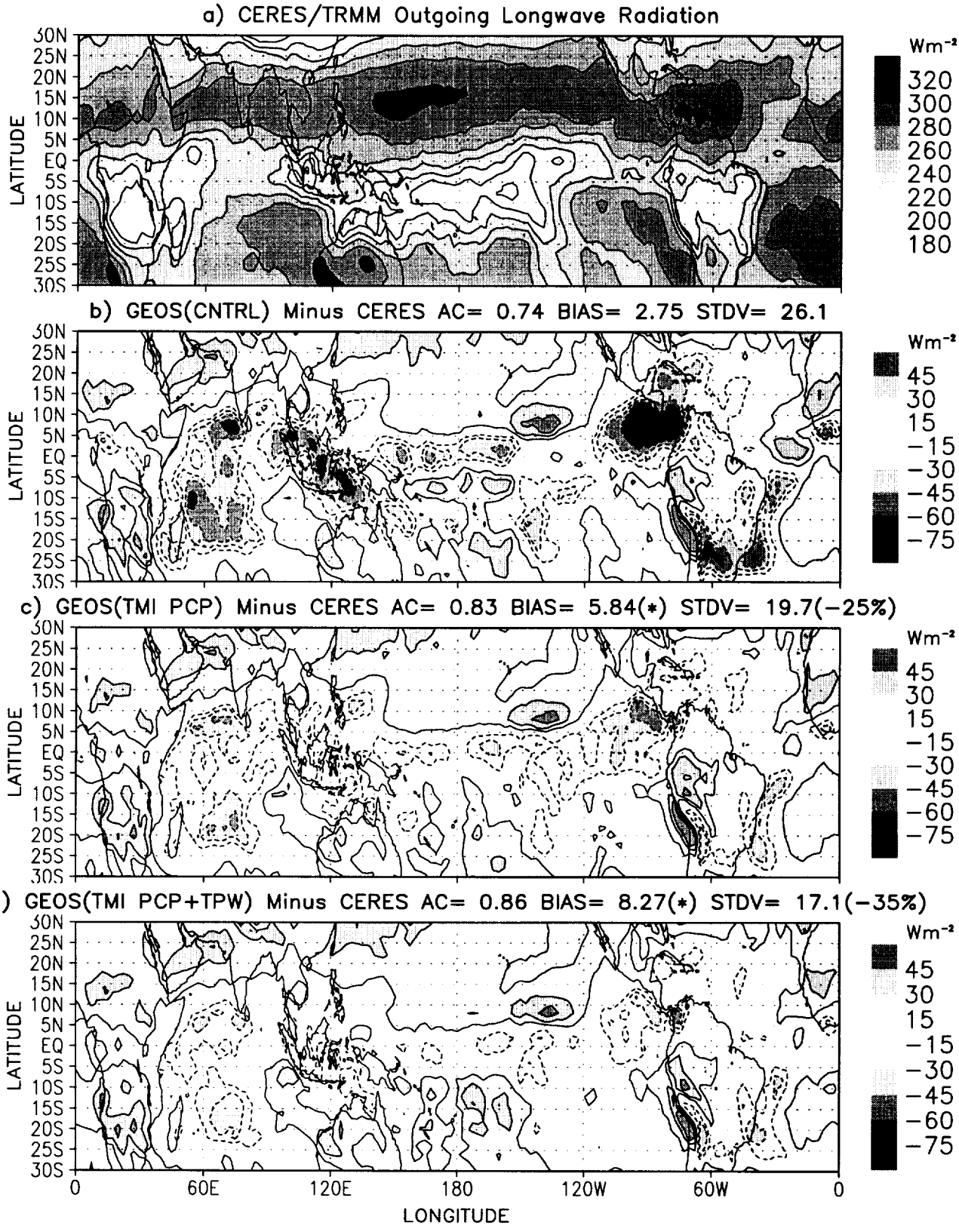

Fig. 3

Impact of Rainfall and TPW Assimilation on OSR: January 1998

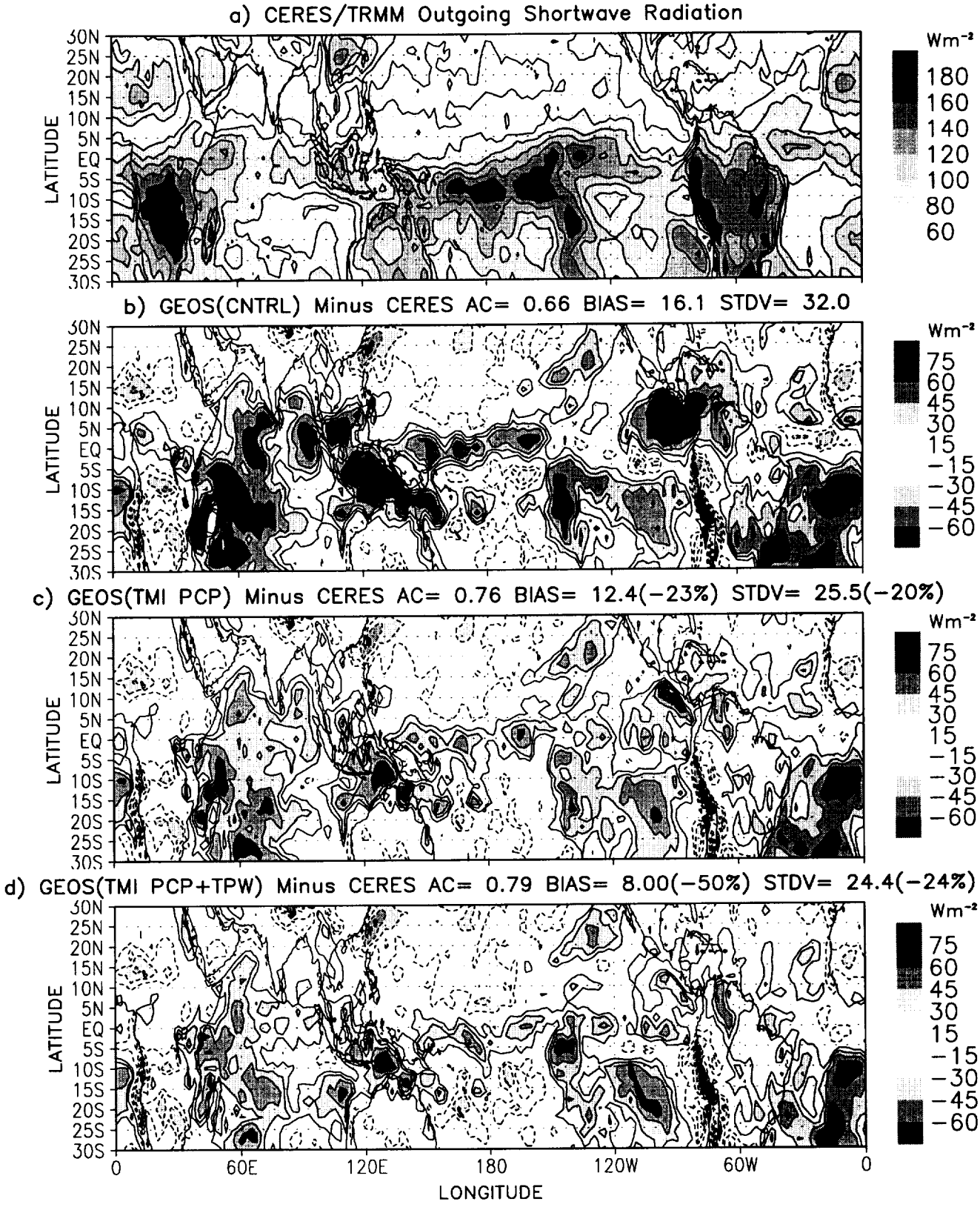

Fig. 4

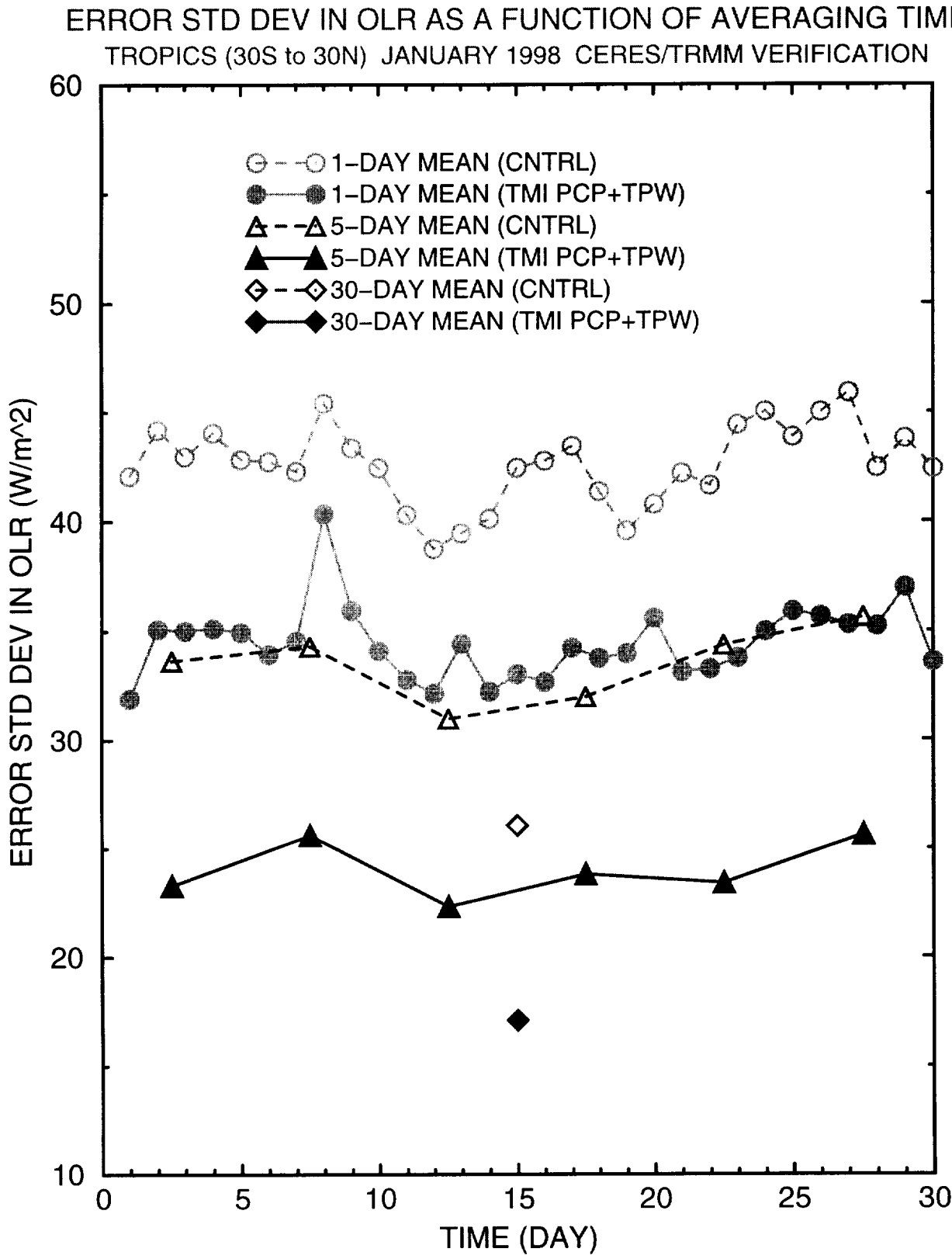
ERROR STD DEV IN OLR AS A FUNCTION OF AVERAGING TIME
TROPICS (30S to 30N) JANUARY 1998 CERES/TRMM VERIFICATION
1-DAY MEAN (CNTRL)
1-DAY MEAN (TMI PCP+TPW)
5-DAY MEAN (CNTRL)
5-DAY MEAN (TMI PCP+TPW)
30-DAY MEAN (CNTRL)
30-DAY MEAN (TMI PCP+TPW)
ERROR STD DEV IN OLR (W/m^2)
TIME (DAY)
60
50
40
30
20
10
0
5
10
15
20
25
30

Fig. 5

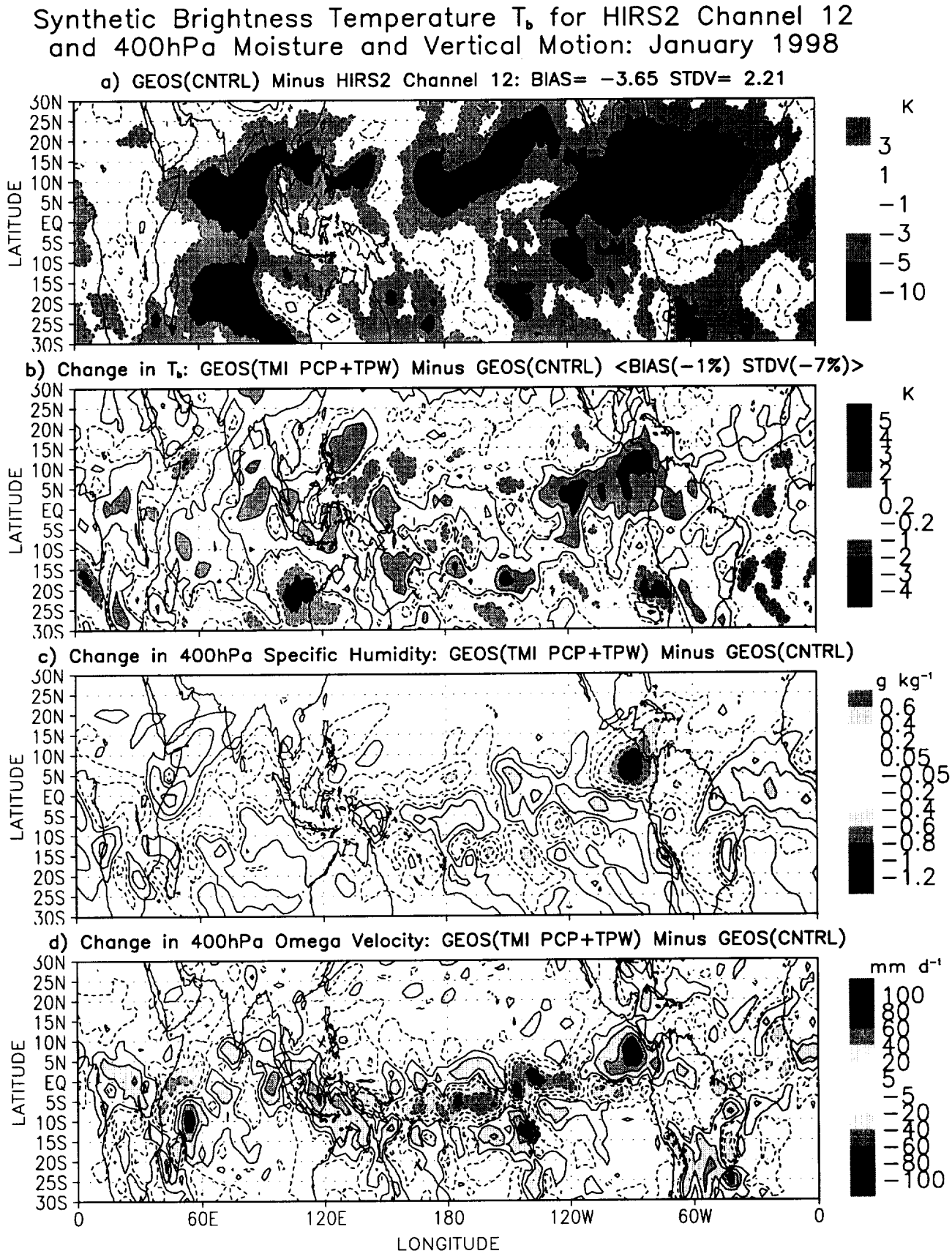
Synthetic Brightness Temperature T_b for HIRS2 Channel 12 and 400hPa Moisture and Vertical Motion: January 1998
a) GEOS(CNTRL) Minus HIRS2 Channel 12: BIAS= −3.65 STDV= 2.21
b) Change in T_b: GEOS(TMI PCP+TPW) Minus GEOS(CNTRL) <BIAS(−1%) STDV(−7%)>
c) Change in 400hPa Specific Humidity: GEOS(TMI PCP+TPW) Minus GEOS(CNTRL)
d) Change in 400hPa Omega Velocity: GEOS(TMI PCP+TPW) Minus GEOS(CNTRL)
LATITUDE
30N 25N 20N 15N 10N 5N EQ 5S 10S 15S 20S 25S 30S
LONGITUDE
0 60E 120E 180 120W 60W 0
K
3 1 −1 −3 −5 −10
K
5 4 3 2 1 0.2 −0.2 −1 −2 −3 −4
g kg⁻¹
0.6 0.4 0.2 0.05 −0.05 −0.2 −0.4 −0.6 −0.8 −1 −1.2
mm d⁻¹
100 80 60 40 20 5 −5 −20 −40 −60 −80 −100

Fig. 6

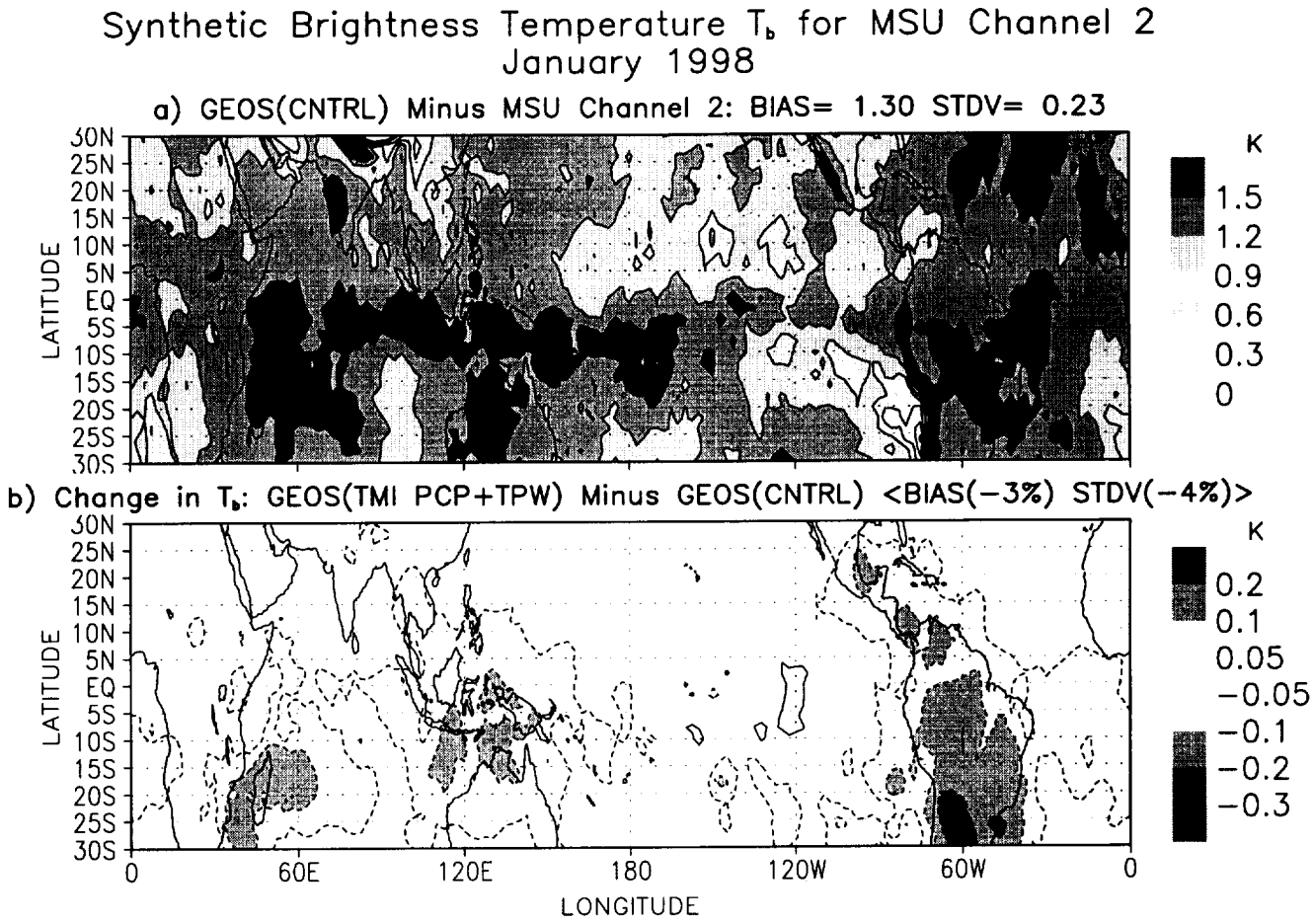
Synthetic Brightness Temperature T_b for MSU Channel 2
January 1998
a) GEOS(CNTRL) Minus MSU Channel 2: BIAS= 1.30 STDV= 0.23
b) Change in T_b: GEOS(TMI PCP+TPW) Minus GEOS(CNTRL) <BIAS(−3%) STDV(−4%)>
LATITUDE
LONGITUDE
30N
25N
20N
15N
10N
5N
EQ
5S
10S
15S
20S
25S
30S
0
60E
120E
180
120W
60W
K
1.5
1.2
0.9
0.6
0.3
0
0.2
0.1
0.05
−0.05
−0.1
−0.2
−0.3

Fig. 7

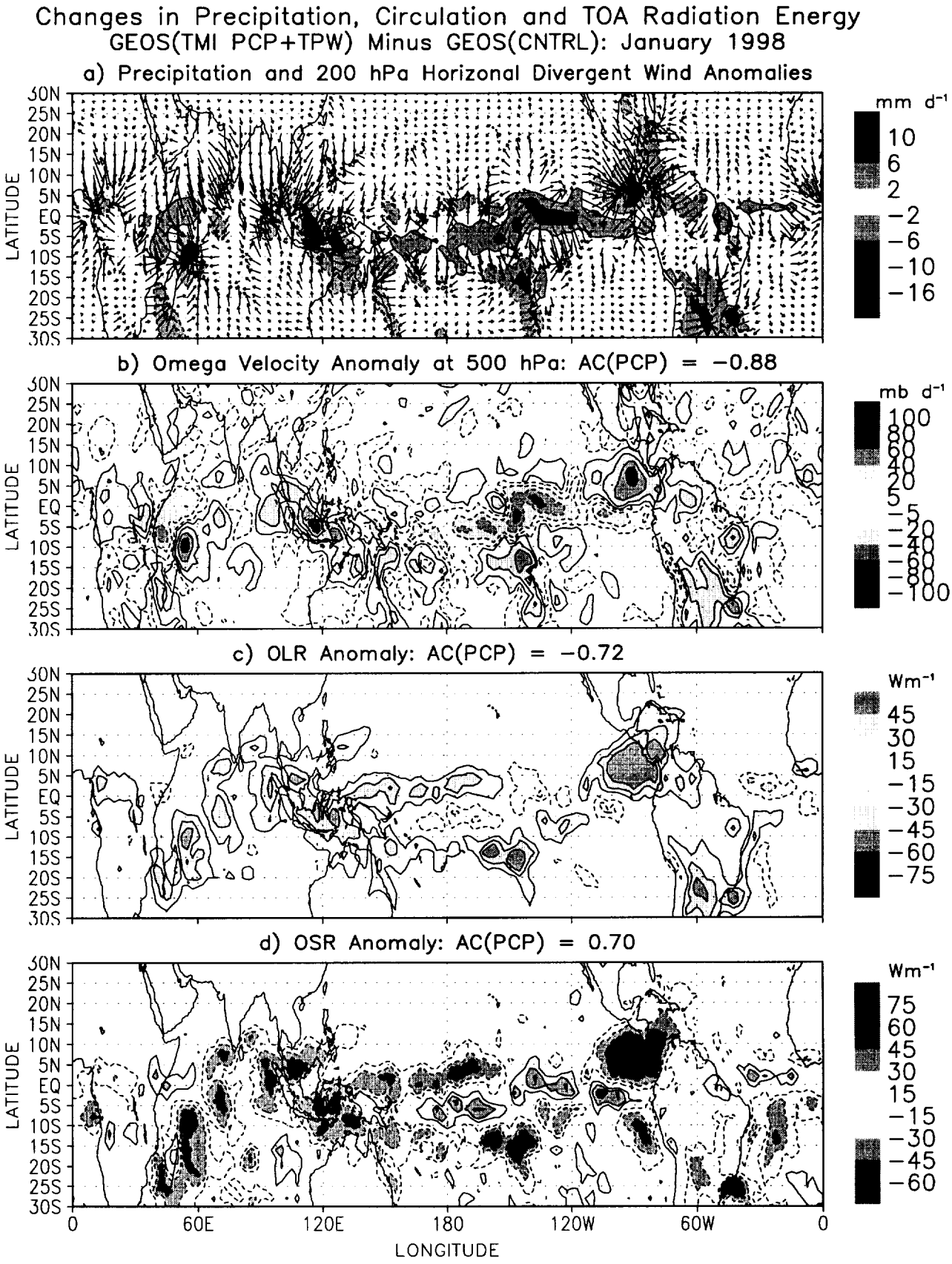
Changes in Precipitation, Circulation and TOA Radiation Energy
GEOS(TMI PCP+TPW) Minus GEOS(CNTRL): January 1998
a) Precipitation and 200 hPa Horizonal Divergent Wind Anomalies
mm d⁻¹
10
6
2
−2
−6
−10
−16
b) Omega Velocity Anomaly at 500 hPa: AC(PCP) = −0.88
mb d⁻¹
100
80
60
40
20
5
−5
−20
−40
−60
−80
−100
c) OLR Anomaly: AC(PCP) = −0.72
Wm⁻¹
45
30
15
−15
−30
−45
−60
−75
d) OSR Anomaly: AC(PCP) = 0.70
Wm⁻¹
75
60
45
30
15
−15
−30
−45
−60
LATITUDE
30N
25N
20N
15N
10N
5N
EQ
5S
10S
15S
20S
25S
30S
0
60E
120E
180
120W
60W
0
LONGITUDE

Fig 8

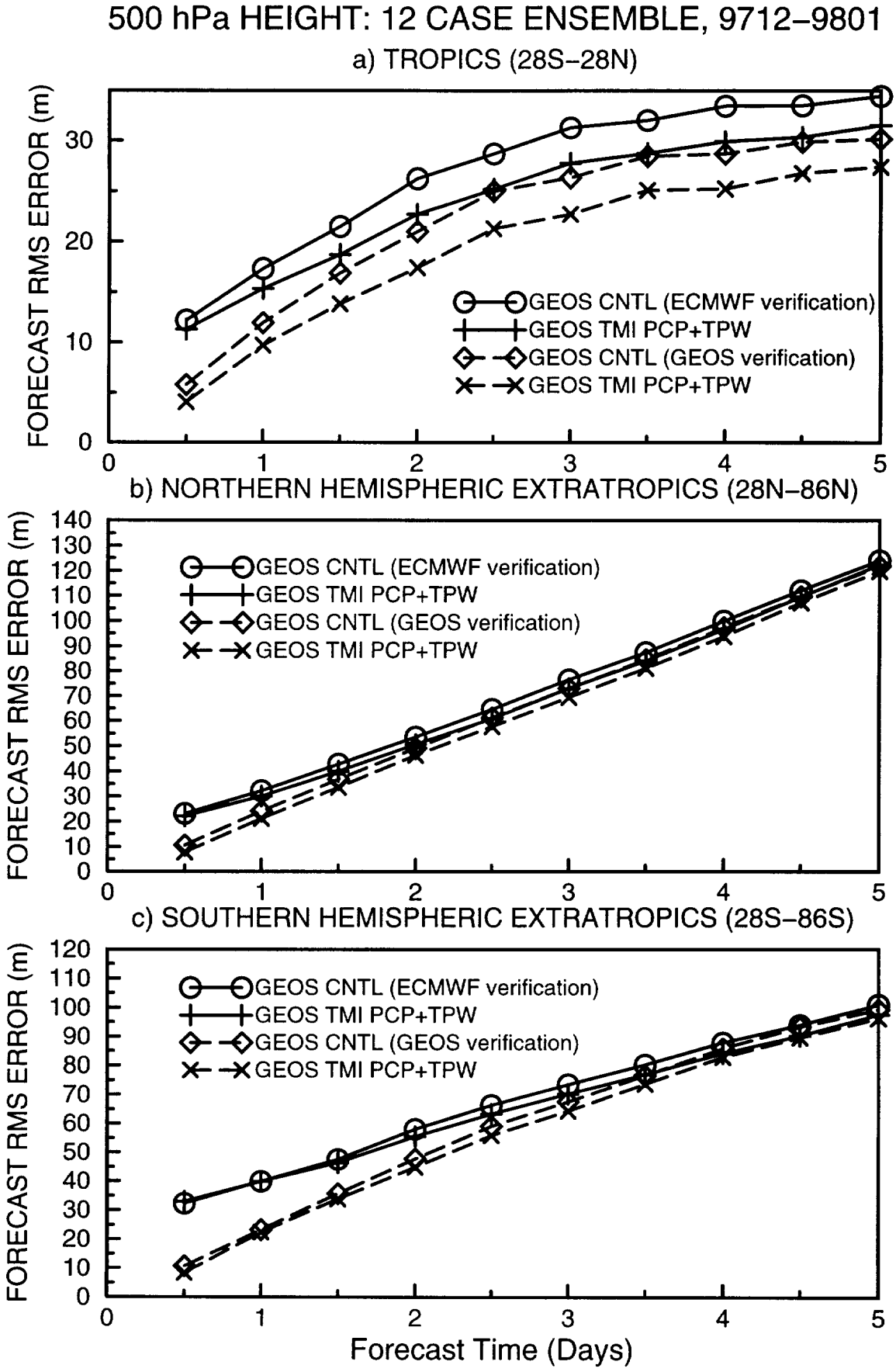
500 hPa HEIGHT: 12 CASE ENSEMBLE, 9712–9801
a) TROPICS (28S–28N)
FORECAST RMS ERROR (m)
0
10
20
30
0
1
2
3
4
5
GEOS CNTL (ECMWF verification)
GEOS TMI PCP+TPW
GEOS CNTL (GEOS verification)
GEOS TMI PCP+TPW
b) NORTHERN HEMISPHERIC EXTRATROPICS (28N–86N)
FORECAST RMS ERROR (m)
0
10
20
30
40
50
60
70
80
90
100
110
120
130
140
0
1
2
3
4
5
GEOS CNTL (ECMWF verification)
GEOS TMI PCP+TPW
GEOS CNTL (GEOS verification)
GEOS TMI PCP+TPW
c) SOUTHERN HEMISPHERIC EXTRATROPICS (28S–86S)
FORECAST RMS ERROR (m)
0
10
20
30
40
50
60
70
80
90
100
110
120
0
1
2
3
4
5
Forecast Time (Days)
GEOS CNTL (ECMWF verification)
GEOS TMI PCP+TPW
GEOS CNTL (GEOS verification)
GEOS TMI PCP+TPW

Fig. 9